XVIII International Conference on Water Resources
CMWR 2010
J. Carrera (Ed)

BASIN-SCALE CO_2 STORAGE CAPACITY ESTIMATES FROM FLUID DYNAMICS

Michael L. Szulczewski, Christopher W. MacMinn and Ruben Juanes*

Massachusetts Institute of Technology
77 Massachusetts Ave, Bldg. 48-319
Cambridge, Massachusetts 02139, USA
e-mail: juanes@mit.edu, web page: http://juanesgroup.mit.edu

Key words: Carbon capture and storage, capacity estimates, capillary trapping, residual trapping, sharp-interface model, analytical solution

Summary. We present an approach for estimating CO_2 storage capacity at the basin scale, based on the principle that the CO_2 plume must be contained in the geologic formation. We develop a sharp-interface mathematical model for the post-injection migration of a plume of CO2 in a deep saline aquifer. We obtain analytic estimates of the maximum plume migration distance and migration time for complete trapping. The model accounts for the combined effect of aquifer slope and regional groundwater flow, whose interplay leads to nontrivial behavior in terms of trapping efficiency. We use our analytical model to estimate the storage capacity from capillary trapping at the geologic basin scale. Since the methodology is based on the fluid dynamics of CO_2 migration, the estimates are basin-specific, and reflect the correct dependencies on the fundamental parameters of the system. We illustrate how to apply the model to a target formation in the Powder River Basin, in the United States.

1 INTRODUCTION

Carbon capture and storage has emerged as one of the key technologies for the abatement of CO_2 emissions, and meeting the energy demands in a carbon constrained world[1]. Deep saline aquifers are attractive geological formations for the injection and long-term storage of CO_2[1]. Even if injected as a supercritical fluid—dense gas—the CO_2 is buoyant with respect to the formation brine. Several trapping mechanisms act to prevent the migration of the buoyant CO_2 back to the surface, and these include[1]: (1) *structural and stratigraphic trapping*: the buoyant CO_2 is kept underground by an impermeable cap rock, either in a closed, non-migrating system (static trapping), or in an open system where the CO_2 migrates slowly (hydrodynamic trapping)[2]; (2) *capillary trapping*: disconnection of the CO_2 phase into an immobile (trapped) fraction[3;4]; (3) *solution trapping*: dissolution of the CO_2 in the brine, possibly enhanced by gravity instabilities[5;6]; and (4) *mineral trapping*: geochemical binding to the rock due to mineral precipitation[7].

The greatest challenge for carbon capture and storage is the massive scale at which it must be deployed to have an impact on atmospheric CO_2 emissions. In the U.S. alone, capturing and storing just 15% of current emissions requires injecting about one gigatonne per year (Gt/yr) of CO_2, a rate of injection that should be sustained for at least several decades. At typical reservoir pressure and temperature conditions, this corresponds to an injection volume on the order of 35 million barrels per day; about twice the oil consumption in the US. Even if injection takes place at dozens of geographically-distributed sites, the storage of this amount of CO_2 must be studied and modeled at the scale of geologic sedimentary basins (hundreds of kilometers), as opposed to the pilot scale (hundreds of meters) or the local reservoir scale (kilometers).

Two fundamental issues are those of injectivity and capacity. These two issues are related, but are different. By capacity we mean the amount of CO_2 that a geologic formation can hold, without consideration of the flow rates at which injection takes place. By (basin-scale) injectivity we mean the maximum flow rate over a given period such that the formation does not fail geomechanically—for instance, by fracturing of the caprock or by activation of previously sealing faults.

Here, we concentrate on capacity estimation. At present, this is done at the basin scale by applying a "storage coefficient", such that the mass of CO_2 that can be injected is given by[8]:

$$\mathcal{C} = \rho_{CO_2} \phi V_T E, \tag{1}$$

where $\mathcal{C}$ is the capacity (mass of CO_2 that can be stored), ρ_{CO_2} is the CO_2 reservoir density, ϕ is the porosity, V_T is the total volume of aquifer (net thickness times area), and E is the storage coefficient. Currently, the storage efficiency coefficient E is obtained as a multiplicative factor, which reduces the capacity due to connate water saturation and loss of swept volume due to buoyancy, stratigraphic heterogeneity, etc.[8]

Here, we provide an alternative definition of the storage efficiency coefficient. We obtain it from the physics of CO_2 migration during and after injection. The principle for capacity estimation is simple: the plume must fit in the geologic basin. We make several simplifying assumptions in order to obtain a migration model that can be studied analytically. While some of these simplifications are fairly restrictive, the methodology allows one to incorporate the different storage mechanisms explicitly, and to quantify the effect of the various physical parameters (fluid viscosities, medium permeability, residual CO_2 saturation, aquifer slope and groundwater flow velocity, etc.) on storage capacity.

2 MATHEMATICAL MODEL OF CO_2 MIGRATION

We are interested in large CO_2 storage projects, and therefore in the evolution of the CO_2 plume at the geologic-basin scale—a schematic of the basin scale geologic setting is shown in figure 1. We assume that the CO_2 is injected simultaneously through a linear arrangement of a large number of wells. The plumes from neighboring wells will merge as the radius of the plumes around wells approaches the inter-well spacing. We model the single resulting plume as two-dimensional in the x-z plane, with some width W in the y-direction equal to the length of the well array.

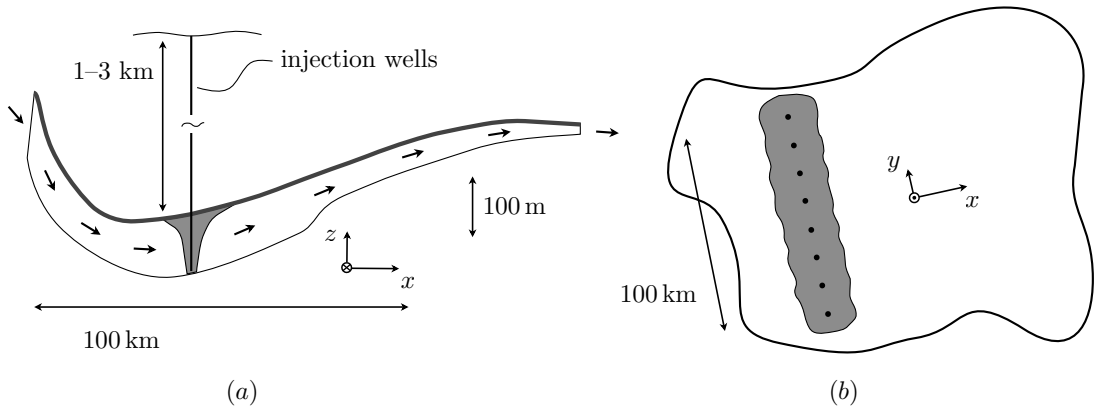

Figure 1: Injection of CO_2 into a saline aquifer at the basin scale. (a) In cross-section, the CO_2 is shown in gray, the groundwater in white, and the caprock as a thick line. Arrows indicate the direction of groundwater flow. Typical horizontal and vertical scales are indicated—note that the vertical scale of the aquifer is greatly exaggerated. (b) From a bird's-eye view, the plumes from the individual wells merge together as the CO_2 spreads away from the well array (black dots).

We take the aquifer to be homogeneous, with an arbitrary tilt angle relative to the horizontal and a net groundwater flow to the right. We take the fluids to be incompressible and Newtonian, with constant and uniform properties within the aquifer. The fraction of pore space occupied by trapped or residual CO_2 after the bulk is displaced is the residual gas saturation, S_{gr}. Similarly, some fraction of pore space may be occupied by immobile groundwater; this is known as the connate water saturation, S_{wc}.

We employ a sharp-interface approximation, neglecting the width of typical gradients in saturation (*i.e.*, the capillary transition zone or "fringe") compared to typical length scales in the horizontal and vertical directions, and we further neglect the capillary pressure compared to typical hydrostatic and viscous pressure drops[9;10]. We divide the domain into three regions of uniform CO_2 and groundwater saturation with sharp interfaces corresponding to saturation discontinuities. As illustrated in figure 2, Region 1 is the mobile plume of CO_2, containing mobile CO_2 with a saturation S_{wc} of connate groundwater; Region 2 is the region from which the plume has receded, containing mobile groundwater with a saturation S_{gr} of trapped CO_2; and Region 3 contains mobile groundwater with no CO_2.

We make the Dupuit or "vertical equilibrium" approximation and neglect the vertical flow velocity compared to the horizontal flow velocity. This is justified when the characteristic vertical length scale is much smaller than the characteristic horizontal one, as is generally the case for aquifers.

The complete derivation of the model under these assumptions is given elsewhere[11;12] The plume migration equation, in dimensionless form, is:

$$\widetilde{\mathcal{R}}\,\frac{\partial \eta}{\partial \tau} + N_f\,\frac{\partial f}{\partial \xi} + N_s\,\frac{\partial}{\partial \xi}\left[(1-f)\eta\right] - N_g\,\frac{\partial}{\partial \xi}\left[(1-f)\eta\,\frac{\partial \eta}{\partial \xi}\right] = 0, \tag{2}$$

where $\eta = h_1/H$ is the dimensionless plume height (normalized by the aquifer thickness H),

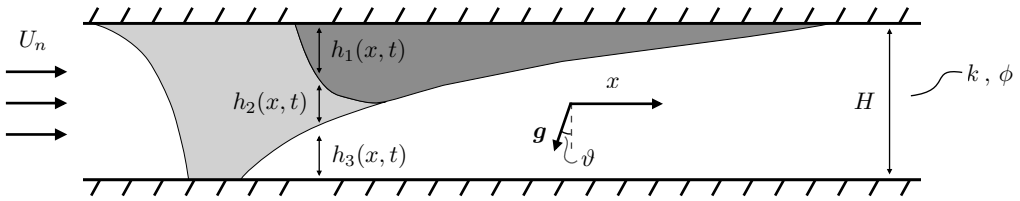

Figure 2: A schematic of the plume during post-injection migration, as the mobile CO_2 is pushed to the right by a combination of groundwater flow and aquifer slope, leaving trapped CO_2 in its wake. We divide the domain into three regions of uniform CO_2 and groundwater saturation, separated by sharp interfaces corresponding to saturation discontinuities. Region 1 (dark gray) has a saturation $1 - S_{wc}$ of mobile CO_2 with a saturation S_{wc} of connate groundwater; Region 2 (light gray) has a saturation S_{gr} of trapped CO_2 and a saturation $1 - S_{gr}$ of mobile groundwater; Region 3 (white) contains only groundwater. The aquifer has a total thickness H, and the thickness of Region i, $i = 1, 2, 3$, is denoted $h_i(x, t)$. Groundwater flows naturally through the aquifer from left to right with velocity U_n; the aquifer has permeability k and porosity ϕ, as well as an arbitrary angle of tilt ϑ measured counterclockwise from the direction of gravity.

$\tau = t/T_c$ is the dimensionless time (normalized by the duration of the injection period, $T_c = T_i$), and $\xi = x/L_c$ is the dimensionless distance (normalized by the characteristic length $L_c = Q_i T_i/2(1 - S_{wc})\phi H$, where Q_i is the integrated volumetric injection flow rate [L^2T^{-1}]). The accumulation coefficient is discontinuous,

$$\widetilde{\mathcal{R}} = \begin{cases} 1 & \text{if } \partial\eta/\partial\tau > 0, \\ 1 - \Gamma & \text{if } \partial\eta/\partial\tau < 0, \end{cases} \tag{3}$$

where $\Gamma = S_{gr}/(1 - S_{wc})$ is the capillary trapping number, which measures the fraction of CO_2 that is left behind at the trail of the plume. The fractional flow function is

$$f(\eta) = \frac{\mathcal{M}\eta}{\mathcal{M}\eta + (1 - \eta)}, \tag{4}$$

where $\mathcal{M} = \lambda_1/\lambda_3$ is the mobility ratio between Regions 1 and 3 (usually much larger than one, due to the high viscosity contrast between brine and CO_2 at reservoir conditions).

The flux terms in equation (2) have the following physical interpretations: the first is advective in nature, capturing the motion of the CO_2 due to groundwater flow through the aquifer; the second is also advective, capturing the motion of the CO_2 due to the tilt of the aquifer; and the third is diffusive, capturing the upward spreading of the CO_2 against the caprock due to buoyancy. The constants N_f (flow number), N_s (slope number), and N_g (gravity number) are given by

$$N_f = \frac{T_c}{T_i}\frac{Q}{Q_i/2}, \quad N_s = \frac{T_c}{L_c}\kappa \sin\vartheta, \quad N_g = \frac{T_c}{L_c}\kappa \cos\vartheta \frac{H}{L_c}. \tag{5}$$

where $Q = U_n H$ is the integrated groundwater flow velocity [L^2T^{-1}], $\kappa = \Delta\rho g k \lambda_1/[(1 - S_{wc})\phi]$ is the intrinsic velocity of buoyancy-driven flow, $\Delta\rho = \rho_w - \rho_g$ is the density difference between the groundwater and the CO_2, g is the force per unit mass due to gravity, and k and ϕ are the intrinsic permeability and porosity of the aquifer, respectively.

Without loss of generality, we choose $N_f \geq 0$—thus groundwater flow is always *to the right* by convention. Aquifer slope can be either positive ($N_s > 0$) for counterclockwise aquifer tilt or negative ($N_s < 0$) for clockwise aquifer tilt.

Numerical simulations of equation (2) show that the essential features of the plume shape and migration are dominated by advective effects and capillary trapping, even for non-negligible values of N_g compared to N_f and N_s[11–14]. Therefore, we neglect the spreading term, which leads to a first-order hyperbolic conservation law.

3 SUMMARY OF ANALYTICAL RESULTS: STORAGE EFFICIENCY

The hyperbolic model can be solved analytically for all combinations of groundwater flow and aquifer slope, accounting fully for the shape of the CO_2 plume at the end of the injection period[15]. A detailed derivation of the analytical solution is given elsewhere[12]; here, we simply summarize the results.

We are primarily interested in the storage efficiency, that is, the volume of CO_2 stored per unit volume of aquifer "used."[8] We define the storage efficiency ε as

$$\varepsilon = \frac{V_{\mathrm{CO_2}}}{V_T} = \frac{Q_i T_i}{H L_T (1 - S_{wc}) \phi}, \tag{6}$$

where $V_{\mathrm{CO_2}}$ is the volume of CO_2 injected and V_T is the total volume of aquifer used; we define V_T to be the total pore volume available for CO_2 storage in a rectangle of thickness H and length L_T, where L_T total extent in the x-direction of the fully trapped CO_2[14]. Taking $\xi_T = L_T/L_c$ and using L_c as defined in §2, we have that $\varepsilon = 2/\xi_T$. The storage efficiency takes a value between 0 and Γ, and is inversely proportional to the dimensionless plume footprint.

The storage efficiency can be readily evaluated from the solution to the migration equation as a function of N_s/N_f, $\mathcal{M}$, and Γ, and this can be done quickly and at high resolution over a large range of parameters owing to the analytical nature of the solution. In figure 3 below, we plot the storage efficiency as a function of N_s/N_f for a typical value $\mathcal{M} = 15$, and several values of Γ.

The storage efficiency always decreases with $\mathcal{M}$—this is because increasing $\mathcal{M}$ strengthens the "tonguing" of the plume during both injection and post-injection migration. Similarly, the storage efficiency always increases with Γ—this is because more CO_2 is left behind upon imbibition, and so the plume becomes fully trapped over a shorter migration distance. Particularly relevant is the fact that the maximum efficiency (which can be obtained analytically and is equal to $\varepsilon_{\max} = \Gamma/\mathcal{M}$) is achieved for a large negative value of $N_s/N_f \approx -\mathcal{M} + 1$, that is, when slope dominates over groundwater flow, and the flow direction is down dip. This is a nontrivial result: figure 3 shows that while the storage efficiency is essentially the same for slope-only ($N_s/N_f = 0$) and flow-only ($N_s/N_f \to \pm\infty$), a gentle down-dip flow can provide a multiple-fold increase in storage efficiency, up to a factor $1/\Gamma$.

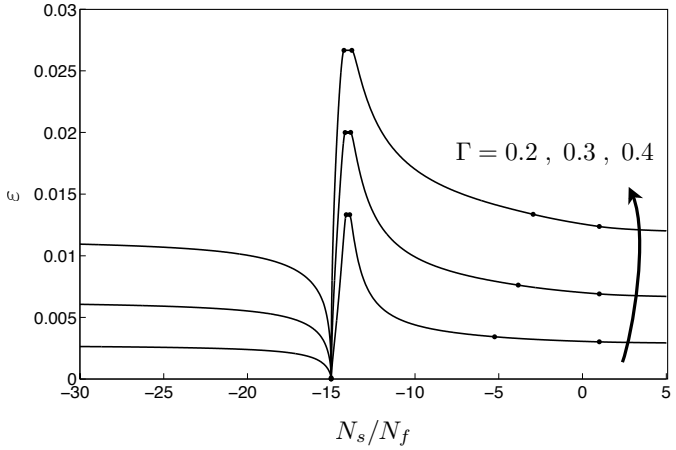

Figure 3: Storage efficiency, ε, as a function of N_s/N_f for several values of Γ, as indicated, at $\mathcal{M} = 15$.

4 APPLICATION TO THE POWDER RIVER BASIN

We apply our model to estimate the storage capacity from capillary trapping of the Fox Hills Sandstone, which extends throughout almost the entire Powder River Basin, between Montana and Wyoming, in the United States[16]. Starting from the Black Hills Uplift in the east, the formation gently dips to the west over most of the basin, but steeply rises before the Bighorn Mountains at the west margin. In the north-south direction, the depth is fairly constant except at the borders of the basin where the formation rises (figure 4). The thickness of the formation is largest in the south and tends to decrease to the north. The Fox Hills Sandstone is Upper Cretaceous in age. Its composition differs in detail in different areas, but in general it consists of commonly massive, fine- to medium-grained sandstone with siltstone and minor shale, which are sometimes interbedded. The formation is conformably overlain by an extensive top seal called the Upper Hell Creek Confining Layer, and conformably overlies marine shale and siltstone. Porosity and permeability data for the formation are very limited, but at least one study indicates a porosity of about 0.2 and a permeability of about 50mD. The flow direction over most of the basin is south to north, as shown in figure 4.

Next, we determine the effective boundary of the Fox Hills Sandstone where the plume is to be contained. An obvious boundary is determined by an outcrop of the formation. We also exclude areas that contain active faults, and those where the caprock contains over 50% sand and may leak CO_2. The resulting effective boundary is shown in figure 4. We also indicate the area that is deep enough for injection, such that the CO_2 is in supercritical state.

The next step is to establish the direction of plume migration. This is based on whether the regional groundwater flow is collinear with aquifer slope or, if it is not, which of the two advection mechanisms (flow or slope) dominate. In the area of interest—the southern section of the formation—the flow direction is roughly perpendicular to the up-dip direction (see figure 4). Based on hydrogeological data, we estimate values of $N_s \approx 0.3$ and $N_f \approx 0.015$. Since $N_s \approx 20N_f$, we choose the up-dip direction as the flow direction, and use a value of $N_s/N_f \to \infty$.

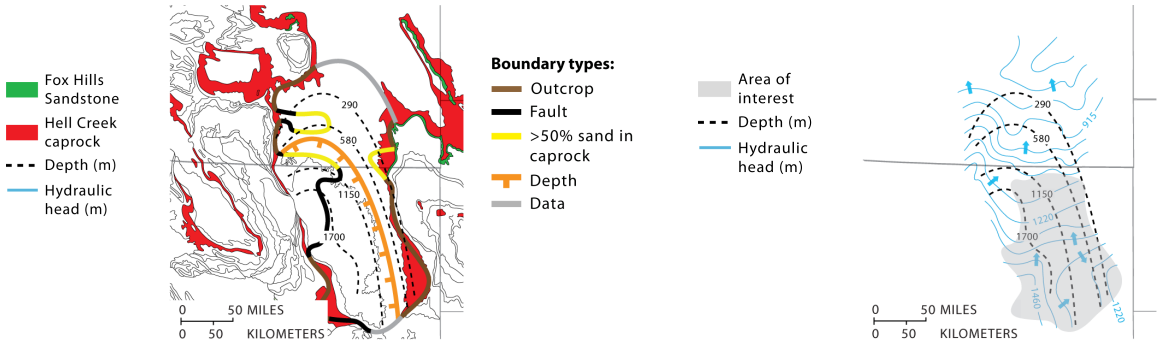

Figure 4: Application of the analytical model to the estimation of storage capacity of the Fox Hills Sandstone, in the Powder River Basin. Left: outcrops of the target formation and the caprock, as well as other effective boundaries that delineate where the CO_2 plume footprint should be contained. Right: Groundwater flow direction, and area (shaded in light gray) where the CO_2 plume will be allowed to migrate.

Table 1: Results from the storage capacity calculation for the Fox Hills Sandstone

Scenario	Efficiency factor	Capacity (gigatons)
Less trapping	0.006	2.3
Average trapping	0.020	7.0
More trapping	0.031	11.0

Other parameters of the model are set by average values in the area of interest: aquifer thickness $H \approx 120$ m, CO_2 density $\rho_{CO_2} \approx 540\ \mathrm{kg\,m^{-3}}$, mobility ratio $\mathcal{M} \approx 5$. We assign values to the remaining variables (connate water saturation S_{wc}, residual CO_2 saturation S_{gr}, endpoint relative permeability k^*_{rg}), based on laboratory data for analogue formations, and according to three different scenarios from less trapping to more trapping [16].

The results from our storage capacity calculation for these three different trapping scenarios are given in table 1. They range from 2 Gt to 11 Gt. It is important to note that only one target formation is considered, and only a fraction of the basin is utilized.

5 CONCLUSIONS

We have presented an approach for estimating CO_2 storage capacity at the basin scale, based on the principle that the CO_2 plume must be contained in the geologic formation. Since the methodology is based on the fluid dynamics of CO_2 migration, the estimates are basin-specific, and reflect the correct dependencies on the fundamental parameters of the system. The model is purely analytical, and accounts for the combined effect of aquifer slope and regional groundwater flow, whose interplay leads to nontrivial behavior in terms of trapping efficiency.

Our model is currently restricted to the mechanism of storage by capillary trapping (residual trapping). It makes many assumptions that allow us to arrive at an analytical model. Some of these assumptions are not always justifiable and therefore does not have universal applicability.

We are currently extending the model to account for dissolution from convective mixing [17], and we are applying the methodology to a number of basins in the continental United States.

References

[1] IPCC. *Special Report on Carbon Dioxide Capture and Storage,* B. Metz, O. Davidson, H. de Coninck, M. Loos and L. Meyer (eds.). Cambridge University Press, 2005.

[2] S. Bachu, W. D. Gunther, and E. H. Perkins. Aquifer disposal of CO_2: Hydrodynamic and mineral trapping. *Energy Conv. Manag.*, 35(4):269–279, 1994.

[3] M. Flett, R. Gurton, and I. Taggart. The function of gas–water relative permeability hysteresis in the sequestration of carbon dioxide in saline formations. In *SPE Asia Pacific Oil and Gas Conference and Exhibition*, Perth, Australia, October 18–20 2004. (SPE 88485).

[4] R. Juanes, E. J. Spiteri, F. M. Orr, Jr., and M. J. Blunt. Impact of relative permeability hysteresis on geological CO_2 storage. *Water Resour. Res.*, 42:W12418, doi:10.1029/2005WR004806, 2006.

[5] J. Ennis-King and L. Paterson. Role of convective mixing in the long-term storage of carbon dioxide in deep saline formations. *Soc. Pet. Eng. J.*, 10(3):349–356, September 2005.

[6] A. Riaz, M. Hesse, H. A. Tchelepi, and F. M. Orr, Jr. Onset of convection in a gravitationally unstable, diffusive boundary layer in porous media. *J. Fluid Mech.*, 548:87–111, 2006.

[7] W. D. Gunter, B. Wiwchar, and E. H. Perkins. Aquifer disposal of CO_2-rich greenhouse gases: Extension of the time scale of experiment for CO_2-sequestering reactions by geochemical modeling. *Miner. Pet.*, 59(1–2):121–140, 1997.

[8] S. Bachu, D. Bonijoly, J. Bradshaw, R. Burruss, S. Holloway, N. P. Christensen, and O. M. Mathiassen. CO_2 storage capacity estimation: methodology and gaps. *Int. J. Greenhouse Gas Control*, 1:430–443, 2007.

[9] J. Bear. *Dynamics of Fluids in Porous Media*. Environmental Science Series. Elsevier, New York, 1972. Reprinted with corrections, Dover, New York, 1988.

[10] Y. C. Yortsos. A theoretical analysis of vertical flow equilibrium. *Transp. Porous Media*, 18: 107–129, 1995.

[11] M. A. Hesse, F. M. Orr, Jr., and H. A. Tchelepi. Gravity currents with residual trapping. *J. Fluid Mech.*, 611:35–60, 2008.

[12] C. W. MacMinn, M. L. Szulczewski, and R. Juanes. CO_2 migration in saline aquifers, I: Capillary trapping under slope and groundwater flow. *J. Fluid Mech.*, 2009. (Submitted).

[13] R. Juanes and C. W. MacMinn. Upscaling of capillary trapping under gravity override: Application to CO_2 sequestration in aquifers. In *SPE/DOE Symposium on Improved Oil Recovery*, Tulsa, OK, April 19–23, 2008. (SPE 113496).

[14] R. Juanes, C. W. MacMinn, and M. L. Szulczewski. The footprint of the CO_2 plume during carbon dioxide storage in saline aquifers: storage efficiency for capillary trapping at the basin scale. *Transp. Porous Media*, 2010. in press, doi:10.1007/s11242-009-9420-3.

[15] C. W. MacMinn and R. Juanes. Post-injection spreading and trapping of CO_2 in saline aquifers: Impact of the plume shape at the end of injection. *Comput. Geosci.*, 13:483–491, doi:10.1007/s10596–009–9147–9, 2008.

[16] M. L. Szulczewski and R. Juanes. A simple but rigorous model for calculating CO_2 storage capacity in deep saline aquifers at the basin scale. *Energy Procedia* (Proc. GHGT-9), 1(1):3307–3314, doi:10.1016/j.egyproc.2009.02.117, 2009.

[17] C. W. MacMinn, M. L. Szulczewski, and R. Juanes. CO_2 migration in saline aquifers, II: Combined capillary and dissolution trapping. *J. Fluid Mech.*, 2010. (In preparation).